Draft version October 18, 2019
Typeset using LaTeX **twocolumn** style in AASTeX62

Detection and characterisation of oscillating red giants: first results from the TESS satellite

Víctor Silva Aguirre,[1] Dennis Stello,[2,3,1] Amalie Stokholm,[1] Jakob R. Mosumgaard,[1] Warrick Ball,[4,1] Sarbani Basu,[5] Lisa Bugnet,[6,7] Derek Buzasi,[8] Tiago L. Campante,[9,10] William J. Chaplin,[4,1] Enrico Corsaro,[11] Yvonne Elsworth,[4,1] Rafael A. García,[6,7] Oliver J. Hall,[4,1] Rasmus Handberg,[1] Thomas Kallinger,[12] Liu Kang,[13] Mikkel N. Lund,[1] Alexey Mints,[14] Benoit Mosser,[15] Zeynep Çelik Orhan,[16] Mathieu Vrard,[9,17] Mutlu Yildiz,[16] Joel C. Zinn,[2,18,17] Sibel Örtel,[16] Paul G. Beck,[19,20,21] Keaton J. Bell,[22,23] Zhao Guo,[24] James S. Kuszlewicz,[25] Charles A. Kuehn,[26] Mia S. Lundkvist,[1] Jamie Tayar,[27,28] Margarida S. Cunha,[9,4] Saskia Hekker,[25,1] Mario J. P. F. G. Monteiro,[9,10] and TESS WG7

[1] *Stellar Astrophysics Centre (SAC), Department of Physics and Astronomy, Aarhus University, Ny Munkegade 120, 8000 Aarhus C, Denmark*
[2] *School of Physics, The University of New South Wales, Sydney NSW 2052, Australia*
[3] *Sydney Institute for Astronomy (SIfA), School of Physics, University of Sydney, NSW 2006, Australia*
[4] *School of Physics and Astronomy, University of Birmingham, Birmingham, B15 2TT, United Kingdom*
[5] *Department of Astronomy, Yale University, New Have, CT 06520, USA*
[6] *IRFU, CEA, Université Paris-Saclay, F-91191 Gif-sur-Yvette, France*
[7] *AIM, CEA, CNRS, Université Paris-Saclay, Université Paris Diderot, Sorbonne Paris Cité, F-91191 Gif-sur-Yvette, France*
[8] *Dept. of Chemistry and Physics, Florida Gulf Coast University, 10501 FGCU Blvd. S., Fort Myers, FL 33965 USA*
[9] *Instituto de Astrofísica e Ciências do Espaço, Universidade do Porto, Rua das Estrelas, 4150-762 Porto, Portugal*
[10] *Departamento de Física e Astronomia, Faculdade de Ciências da Universidade do Porto, Rua do Campo Alegre, s/n, 4169-007 Porto, Portugal*
[11] *INAF Osservatorio Astrofisico di Catania, Via S. Sofia, 78, 95123 Catania, Italy*
[12] *Institut für Astrophysik, Universität Wien, Türkenschanzstrasse 17, 1180 Vienna, Austria*
[13] *Department of Astronomy, Beijing Normal University, 100875 Beijing, PR China*
[14] *Leibniz-Institut für Astrophysik Potsdam (AIP), An der Sternwarte 16, 14482 Potsdam, Germany*
[15] *LESIA, Observatoire de Paris, Université PSL, CNRS, Sorbonne Université, Université de Paris, 92195 Meudon, France*
[16] *Department of Astronomy and Space Sciences, Science Faculty, Ege University, 35100, Bornova, İzmir, Turkey*
[17] *Department of Astronomy, The Ohio State University, 140 West 18th Avenue, Columbus OH 43210, USA*
[18] *Kavli Institute for Theoretical Physics, University of California, Santa Barbara, CA 93106, USA*
[19] *Institute of Physics, Karl-Franzens University of Graz, NAWI Graz, Universitätsplatz 5/II, 8010 Graz, Austria*
[20] *Instituto de Astrofísica de Canarias, E-38200 La Laguna, Tenerife, Spain*
[21] *Departamento de Astrofísica, Universidad de La Laguna, E-38206 La Laguna, Tenerife, Spain*
[22] *DIRAC Institute, Department of Astronomy, University of Washington, Seattle, WA 98195-1580, USA*
[23] *NSF Astronomy and Astrophysics Postdoctoral Fellow and DIRAC Fellow*
[24] *Center for Exoplanets and Habitable Worlds, Department of Astronomy and Astrophysics, 525 Davey Laboratory, The Pennsylvania State University, University Park, PA16802, USA*
[25] *Max Planck Institute for Solar System Research, Justus-von-Liebig Weg 3, D-37077 Göttingen, Germany*
[26] *Department of Physics and Astronomy, University of Northern Colorado, Greeley, CO 80639, USA*
[27] *Institute for Astronomy, University of Hawaii, 2680 Woodlawn Drive, Honolulu, Hawaii 96822, USA*
[28] *Hubble Fellow*

(Received January 1, 2018; Revised January 7, 2018; Accepted October 18, 2019)

Submitted to ApJL

ABSTRACT

Since the onset of the 'space revolution' of high-precision high-cadence photometry, asteroseismology has been demonstrated as a powerful tool for informing Galactic archaeology investigations. The launch of the NASA TESS mission has enabled seismic-based inferences to go full sky – providing a

Corresponding author: Víctor Silva Aguirre
victor@phys.au.dk

clear potential for large ensemble studies of the different Milky Way components. Here we show the first asteroseismic ensemble study of red giant stars observed by TESS to demonstrate its potential for investigating the Galaxy. We use a modest sample of stars for which we measure their global asteroseimic observables and estimate their fundamental stellar properties, such as radius, mass, and age. Clear improvements are seen in the uncertainties of our estimates when combining seismic observables from TESS with astrometric measurements from the Gaia mission compared to when the seismology and astrometry are applied separately. Specifically, when combined we find stellar radii to a precision of a few percent, masses to 5-10% and ages to the 20% level. This is comparable to the precision typically obtained using *Kepler* data.

Keywords: asteroseismology — stars: fundamental parameters — techniques: photometric

1. INTRODUCTION

Asteroseismology of red giant stars has been one of the major successes of the CoRoT (Baglin et al. 2006) and *Kepler* (Borucki et al. 2010) missions. The unambiguous detection of non-radial oscillations (De Ridder et al. 2009) has fundamentally widened our understanding of the inner workings of red giants, including the conditions in their core (e.g., Bedding et al. 2011) and their rotation profiles (e.g., Beck et al. 2012). The observed frequency spectra have allowed the determination of the physical properties of thousands of red giants to an unprecedented level of precision (e.g., Miglio et al. 2013), paving the way for the irruption of asteroseismology as a powerful tool for Milky Way studies and Galactic archaeology (Casagrande et al. 2016; Silva Aguirre et al. 2018; Sharma et al. 2019). The *Transiting Exoplanet Survey Satellite* (TESS, Ricker et al. 2015) is on the path of continuing this legacy with its all-sky survey that is expected to increase the number of detected oscillating red giants by an order of magnitude compared to the tens of thousands reported by its predecessors CoRoT and *Kepler*.

In the nominal TESS mission, the northern and southern hemispheres are each observed during thirteen 27-day-long sectors, and most (92%) of the surveyed sky will be monitored for just 1-2 sectors. Except for the 20,000 targets pre-selected in each sector for 2-min cadence observations, all stars are observed as part of the full frame images obtained in 30-min cadence, similar to the long cadence sampling of the *Kepler* satellite. The length of the observations sets the lower limit on the oscillation frequencies one can resolve, and the sampling sets the upper frequency limit. We know from previous *Kepler* observations that one month of long cadence data should be well suited to detect oscillations in the low red giant branch (RGB) and sufficient to measure the global oscillation properties charaterising the frequency spectrum, in particular, its frequency of maximum power, $\nu_{\rm max}$ and the frequency separation between overtone modes, $\Delta\nu$ (Bedding et al. 2010). These in turn can be used in combination with complementary data such as the effective temperature, $T_{\rm eff}$, the relative iron abundance, [Fe/H], and parallax, to obtain precise stellar properties (including ages) when applying asteroseismic-based grid modelling approaches (see e.g., Rodrigues et al. 2017; Pinsonneault et al. 2018).

Due to the large sky coverage, approximately 97% of asteroseismic detections in red giants from the TESS nominal mission data are expected to come from stars observed for only one or two sectors[1]. Here we set out to explore the capability of TESS to detect the oscillations in giants ranging from the base of the red giant branch to the red clump, determine their stellar properties, and use that to assess the prospects for Galactic archaeology studies using one to two sectors of TESS data.

2. TARGET SELECTION

Our goal is to have a representative sample of giants including the types of stars in which we can expect to detect oscillations from one sector long-cadence TESS data. We selected red giant candidates observed during sectors 1 and/or 2 that were deemed viable for asteroseismic detections according to their predicted properties based on the *Hipparcos* catalogue (Van Leeuwen 2007). We first estimated the stellar $T_{\rm eff}$ and luminosity using $B-V$ color, V-band, and *Hipparcos* parallax, and the color-temperature and bolometric correction relations of Flower (1996). We then obtained a prediction of $\nu_{\rm max}$ assuming a mass of 1.2 $M_{\odot}$, which is representative of a typical red giant as observed by *Kepler* (and unlikely to be more than a factor of two from the true value of each star, Yu et al. (2018)). We note that one of our targets (TIC 129649472) is a known exoplanet host star recently analysed by Campante et al. (2019).

To ensure that the selected targets were amenable to asteroseismic detection from one sector of 30-min cadence data, we required they would have an expected $\nu_{\rm max}$ in the range 30-220μHz and $T_{\rm eff}$ in the typical range

[1] TESS GI proposal

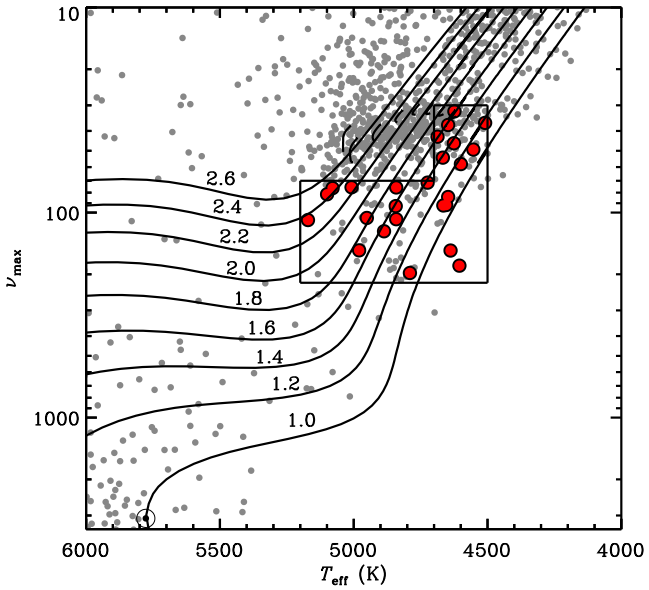

Figure 1. 'Asteroseismic HR diagram' showing $\nu_{\rm max}$ instead of luminosity. Red dots show the selected targets inside the black selection box. For reference, the Sun is shown as well as all *Hipparcos* stars brighter than 6th magnitude (grey dots). Solar metalicity MESA tracks are shown to guide the eye (pre- and post- helium core-ignition phases are shown separately).

of red giants of 4500-5200 K. In addition, we applied a more narrow $T_{\rm eff}$ range of 4500-4700 K for the stars with $\nu_{\rm max}$ between 30μHz and 70μHz, to avoid having red clump stars dominating our sample. The resulting sample of stars span evolutionary phases from the base of the red giant branch to the red giant branch bump, as well as some clump stars.

From this sample, we selected the 25 brightest targets for light curve extraction and asteroseismic analysis. The faintest stars in our sample turned out to be ∼6-7th magnitude in V band. Under the assumption that the photometric performance of TESS is similar to *Kepler's*, apart from its smaller aperture, this magnitude limit is equivalent to 11-12th magnitude for *Kepler*. Because single-quarter observations from *Kepler's* second life, K2, showed no oscillation detection bias for red giants brighter than around 12th magnitude (Stello et al. 2017) we would expect to detect oscillations in all 25 giants with TESS.

Figure 1 illustrates the location of the selected stars in the HR-diagram and the applied selection criteria. We confirmed that the stars were in the desired sectors using the Web TESS Viewing tool (WTV)[2].

3. DATA PROCESSING AND ASTEROSEISMIC ANALYSIS

The stars selected were included in an early release of processed data from the TASOC pipeline[3]. The processing combined the methodology from the K2P2 pipeline (Lund et al. 2015) for extracting the flux from target pixel data with the KASOC filter for systematics correction (Handberg & Lund 2014). The resulting TASOC light curves were high-pass filtered using a filter width of 4 days, corresponding to a cut-off frequency of approximately 3μHz , and 4σ outliers were removed. Finally, we used linear interpolation to fill gaps that lasted up to three consecutive cadences and derived the Fourier transforms (power frequency spectra) of each light curve.

The light curves for the seven stars observed in both sectors were merged. To follow the approach anticipated for the millions of light curves from the TESS full frame images in the future, we first applied the neural network-based detection algorithm by Hon et al. (2018) resulting in detection of oscillations in the power spectra of all stars except one. The non-detection is listed as an A2 dwarf and a 'Visual Double' in the University of Michigan Catalogue of two-dimensional spectral types for the HD stars (Houk (1994)), and hence possibly too hot to show solar-like oscillations, or potentially contaminated. For the current test case, the number of stars was small enough that we visually checked the results, which confirmed all detections and the non-detection. The power spectra of a representative sample of the stars are shown in Figure 2 showing clear oscillation excess power and the frequency pattern required to measure both $\nu_{\rm max}$ and $\Delta\nu$.

The neural network also supplies a rough estimate for $\nu_{\rm max}$, which we provided as a prior to 13 independent groups analysing the power spectra to extract high-precision values of both $\nu_{\rm max}$, $\Delta\nu$, and their respective uncertainties using their preferred method. These methods have been thoroughly tested and described in the literature (see e.g., Huber et al. 2009; Gaulme et al. 2009; Hekker et al. 2010; Mathur et al. 2010; Mosser et al. 2011; Kallinger et al. 2012; Corsaro & De Ridder 2014; Davies et al. 2016; Campante et al. 2017; Zinn et al. 2019).

From the 13 independent determinations of the global asteroseismic parameters we adopted as central reference value for $\Delta\nu$ and $\nu_{\rm max}$ the results from the `PGA` pipeline (Gaulme et al. 2009), as it was the method that

[2] https://heasarc.gsfc.nasa.gov/cgi-bin/tess/webtess/wtv.py

[3] T'DA Data Release Notes - Data Release 3 for TESS Sectors 1+2 (https://doi.org/10.5281/zenodo.2510028)

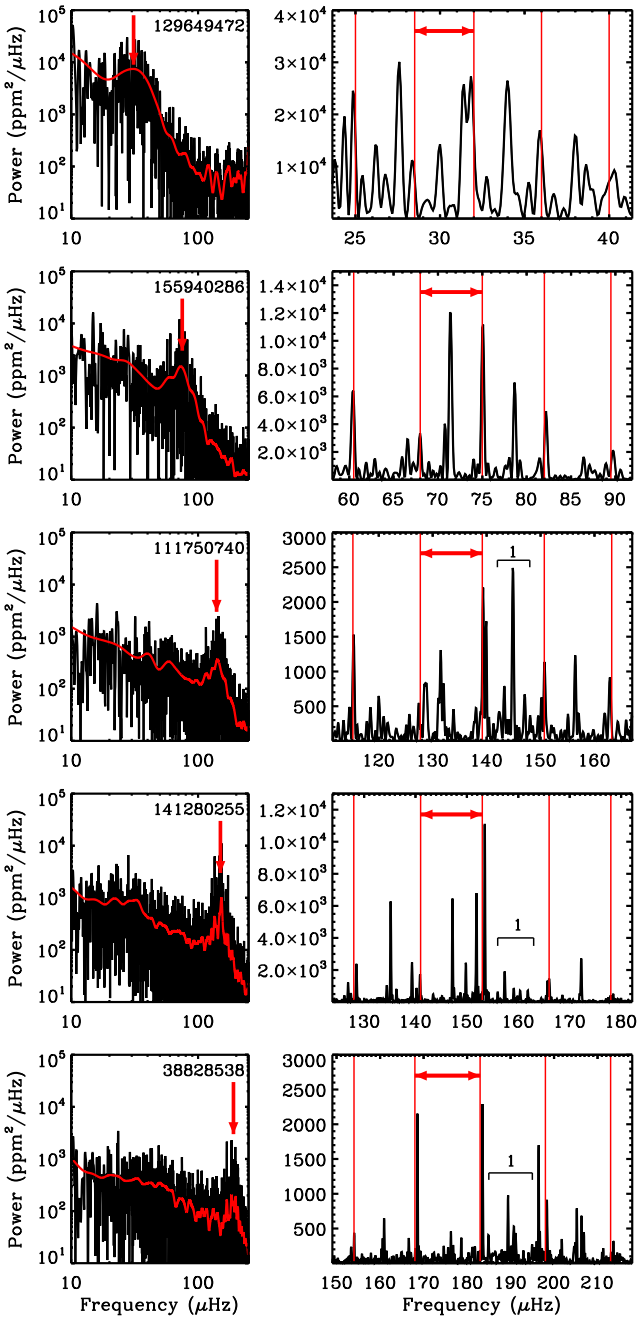

Figure 2. Power spectra sample of our targets representative of the $\nu_{\rm max}$ range that they cover from around the red clump (top) to the low luminosity red giant branch (bottom). *Left*: Spectra shown in log-log space (smoothed in red) showing the location of the oscillation power excess, $\nu_{\rm max}$, indicated by red arrows on top of a frequency-dependent granulation background and flat white noise component. *Right*: Close-up of spectra showing rough locations of the radial modes to guide the eye (red vertical lines) and their average separation, $\Delta\nu$ (red horizontal arrows). In the three bottom panels multiple dipole ($l = 1$) mixed modes are resolved in between consecutive radial modes as indicated by the black brackets.

on average was closest to the ensemble mean after applying a 2-σ outlier rejection. Uncertainties in the global asteroseismic parameters obtained by the selected pipeline are at the 1.9% and 2.4% level for $\Delta\nu$ and $\nu_{\rm max}$ respectively. These uncertainties are of comparable magnitude to those obtained from a single campaign with the K2 mission (see appendix in Stello et al. 2017) and about twice as large as those extracted from 50 days of *Kepler* observations (see Figs. 3 and 4 in Hekker et al. 2012). We report the central values and statistical uncertainties in $\Delta\nu$ and $\nu_{\rm max}$ for all targets in Table 1.

For each star, we take into account the scatter across the different methods by adding in quadrature the standard deviation among the central values retained after the 2-σ outlier rejection procedure to the formal uncertainty reported by the selected reference method. This consolidation process yields median uncertainties of 3.9% in $\Delta\nu$ and 2.6% in $\nu_{\rm max}$, where the individual contribution arising from this systematic component to the total uncertainty is listed in Table 1. We note that we could decrease the level of uncertainties resulting from our 'blind' statistical consolidation approach by for example checking the $\Delta\nu$ and $\nu_{\rm max}$ results against the power spectra and/or échelle diagrams (see Fig. 5 in Stello et al. 2011). However, we want to draw a realistic picture of the uncertainties one can expect when dealing with large ensembles of stars (as expected from TESS) where detailed 'boutique' analysis/checking on a star-by-star basis is not practically feasible. Hence, our quoted uncertainties are conservative but representative for analysis of TESS red giants where several pipelines are involved.

4. DERIVED STELLAR PROPERTIES

We have determined stellar properties for a subsample of 17 stars that had measurements of effective temperature and chemical composition available in the literature. This information was complemented with parallaxes from Gaia DR2 (Gaia Collaboration et al. 2018) and the use of the asteroseismic scaling relations:

$$\left(\frac{\Delta\nu}{\Delta\nu_\odot}\right)^2 \simeq \frac{\overline{\rho}}{\overline{\rho}_\odot} \qquad (1)$$

$$\left(\frac{\nu_{\rm max}}{\nu_{\rm max,\odot}}\right) \simeq \frac{M}{M_\odot}\left(\frac{R}{R_\odot}\right)^{-2}\left(\frac{T_{\rm eff}}{T_{\rm eff,\odot}}\right)^{1/2}, \qquad (2)$$

where we adopted $\Delta\nu_\odot = 135.5$ (μHz) and $\nu_{\rm max,\odot} = 3140$ (μHz) as obtained by our reference pipeline from the analysis of solar data. Seven teams independently applied grid-based modelling pipelines based on stellar evolution models or isochrones to determine the main physical properties of the targets (see Basu et al. 2012;

Silva Aguirre et al. 2015; Rodrigues et al. 2017; Mints & Hekker 2018; Yıldız et al. 2019, and references therein). When matching the models to the atmospheric properties and the global asteroseismic parameters $\Delta\nu$ and $\nu_{\rm max}$ the pipelines yielded radius, mass, and age for the targets with median uncertainties of ∼5%, ∼12%, and ∼41%, respectively. These statistical uncertainties are of the same magnitude to those obtained with the K2 mission (Sharma et al. 2019), as expected from the similar resulting errors in the global seismic parameters described in Section 3, and about a factor of two larger than what can be achieved with the full duration of the *Kepler* observations (Pinsonneault et al. 2018).

In addition to the asteroseismic information, five of the pipelines can include Gaia DR2 parallaxes coupled with Tycho-2 (Høg et al. 2000) observed V-magnitudes in their fitting algorithm to further constrain the stellar properties. The resulting uncertainties decrease to a level of ∼3% in radius, ∼7% in mass, and ∼22% in age. This level of precision resembles that obtained with the use of the full length of asteroseismic observations from the nominal *Kepler* mission, and emphasizes the potential of TESS for Galactic studies using red giants given its larger sky coverage, simple and reproducible selection function, and order of magnitude higher expected yield of asteroseismic detections than any other previous mission.

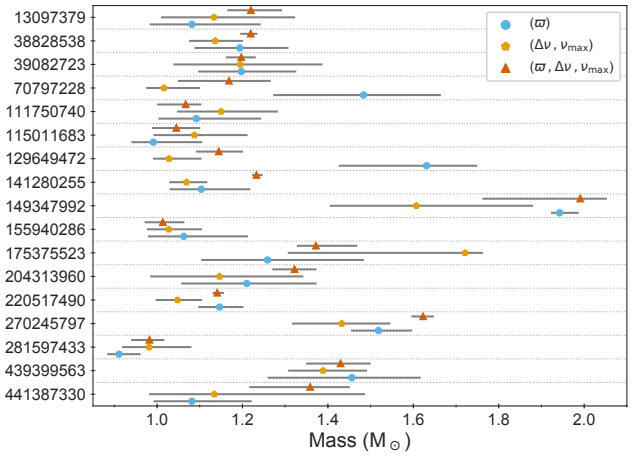

Figure 3. Stellar masses obtained with `BASTA` when fitting different combinations of input parameters: Gaia DR2 parallax and V-band magnitude (ϖ), global asteroseismic parameters ($\Delta\nu$,$\nu_{\rm max}$), and all combined (ϖ ,$\Delta\nu$,$\nu_{\rm max}$). Effective temperature and composition are also fitted in all cases. See text for details.

To further illustrate the gain in precision obtained when combining the global asteroseismic properties with the astrometric solutions from Gaia, Fig. 3 shows the masses obtained with one of the pipelines (`BASTA`, Silva Aguirre et al. 2015) when fitting different combinations of input parameters. The figure includes the case when, in addition to the atmospheric properties, only the Gaia DR2 parallax and observed V-band magnitude are included. For the majority of the targets the results are consistent across the three sets within their formal statistical uncertainties, with a clear improvement in precision when asteroseismic information and parallax are simultaneously included in the fit. Two targets (TIC 70797228 and TIC 129649472) present a larger disagreement between the masses obtained with parallax and the seismic set ($\Delta\nu$,$\nu_{\rm max}$). The parallax-only solution determines a surface gravity that is not compatible with the seismic one, and via the scaling relation (Eq. 2) it predicts a distribution of $\nu_{\rm max}$ that includes the measurements from TESS only in its wings. This effects causes the discrepancy in the predicted masses and explains the existence of an intermediate solution when all the observables (ϖ ,$\Delta\nu$,$\nu_{\rm max}$) are considered in the fit.

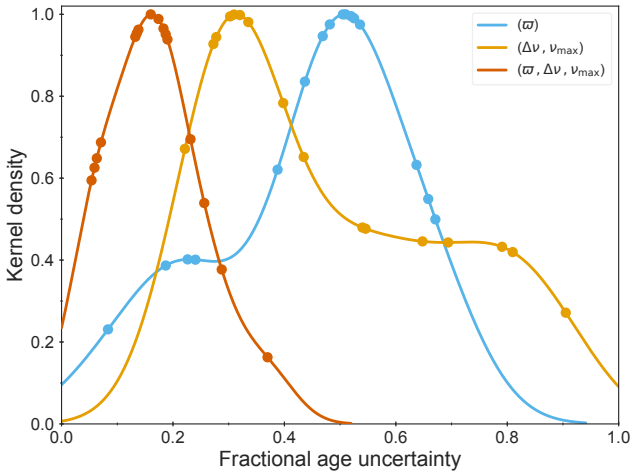

Figure 4. Distribution of fractional age uncertainties for our sample of stars determined by the `BASTA` pipeline fitting different combinations of available observables. The points indicate the individual values used to construct the Gaussian kernel density estimation. For better visualization we have excluded TIC 175375523 from the figure. See text for details.

In Fig. 4 we plot the distribution of fractional age uncertainties obtained with `BASTA` for the three considered cases of input, showing the impact in the obtained statistical age uncertainties of including different combinations of input. We note that for visualization purposes we have excluded the target TIC 175375523 from the figure as its fractional age uncertainty obtained with ($\Delta\nu$,$\nu_{\rm max}$) exceeds one. Its resulting age distribution is bimodal in this set as both RGB and clump models can

reproduce the observations, but the inclusion of parallax information favours the red giant branch solution and explains the $\sim 20\%$ statistical uncertainty reported in Table 1.

Our stellar ages at the 20% level are significantly more precise than what is obtained by data driven and neural network methods trained using asteroseismic ages from *Kepler* (above the 30% level, see e.g., Mackereth et al. 2019). A summary of the measured and derived stellar properties for our targets can be found in Table 1, where we have listed the central values and statistical uncertainties obtained with the `BASTA` pipeline, and determined the systematic contribution as the standard deviation across the results reported by all pipelines.

5. CONCLUSIONS

We presented the first ensemble analysis of red giants stars observed with the TESS mission. We selected a sample of 25 stars where we expected to detect oscillations based on their magnitude and parallax value, and analysed the extracted light curves in search for asteroseismic signatures in the power spectra. Our main findings can be summarized as follows:

- We detected oscillations in all the stars (except one that was likely incorrectly listed as a red giant). Despite the modest number of stars in our sample, our detection yield supports that the TESS photometric performance is similar to that of *Kepler* and K2 apart from its smaller aperture.

- Individual pipelines retrieve the global asteroseismic parameters with uncertainties at the $\sim$2% level in $\Delta\nu$ and $\sim$2.5% in $\nu_{\rm max}$, which respectively increase to $\sim$4% and $\sim$3.5% when we take into account the scatter across results. We consider these uncertainties to be representative for the forthcoming ensemble analysis of TESS targets observed in 1-2 sectors, as individual validation of the results will not be feasible due to the large number of targets observed.

- Grid-based modelling techniques applying asteroseismic scaling relations were used to retrieve stellar properties for the 17 targets with spectroscopic information. Radii, masses, and ages were obtained with uncertainties at the 5%, 12%, and 41% level, and decrease to 3%, 7%, and 22% when parallax information from Gaia DR2 is included.

The expected number of red giants with detected oscillations by TESS ($\sim$500,000) greatly surpasses the final yield of *Kepler* ($\sim$20,000, Hon et al. (2019)). In this respect, the combination of TESS observations, Gaia astrometry, and large scale spectroscopic surveys holds a great potential for studies of Galactic structure where precise stellar properties (particularly ages) are of key importance. We note that the recently approved extended TESS mission will change the long cadence of observations to 10 minutes, making it possible to detect oscillations of stars of smaller radii using full frame images. This will enable more rigorous investigations of the asteroseismic mass scale for giants when anchored to empirical mass determinations (e.g., from eclipsing binaries) of turn-off and subgiant stars.

This paper includes data collected by the TESS mission, which are publicly available from the Mikulski Archive for Space Telescopes (MAST). Funding for the TESS mission is provided by NASAs Science Mission directorate.

REFERENCES

Alves, S., Benamati, L., Santos, N. C., et al. 2015, Monthly Notices of the Royal Astronomical Society, 448, 2749

Baglin, A., Michel, E., Auvergne, M., & Team, C. 2006, in Proceedings of SOHO 18/GONG 2006/HELAS I, 34

Basu, S., Verner, G. A., Chaplin, W. J., & Elsworth, Y. 2012, ApJ, 746, 76

Beck, P. G., Montalban, J., Kallinger, T., et al. 2012, Nature, 481, 55

Bedding, T. R., Huber, D., Stello, D., et al. 2010, ApJL, 713, L176

Bedding, T. R., Mosser, B., Huber, D., et al. 2011, Nature, 471, 608

Borucki, W. J., Koch, D., Basri, G., et al. 2010, Science, 327, 977

Campante, T. L., Veras, D., North, T. S. H., et al. 2017, Monthly Notices of the Royal Astronomical Society, 469, 1360

Campante, T. L., Corsaro, E., Lund, M. N., et al. 2019, arXiv e-prints, arXiv:1909.05961

Casagrande, L., Silva Aguirre, V., Schlesinger, K. J., et al. 2016, Monthly Notices of the Royal Astronomical Society, 455, 987

Corsaro, E., & De Ridder, J. 2014, Astronomy and Astrophysics, 571, A71

da Silva, R., Milone, A. d. C., & Rocha-Pinto, H. J. 2015, Astronomy and Astrophysics, 580, A24

Davies, G. R., Silva Aguirre, V., Bedding, T. R., et al. 2016, Monthly Notices of the Royal Astronomical Society, 456, 2183

De Ridder, J., Barban, C., Baudin, F., et al. 2009, Nature, 459, 398

Flower, P. J. 1996, ApJ, 469, 355

Gaia Collaboration, Katz, D., Antoja, T., et al. 2018, Astronomy and Astrophysics, 616, A11

Gaulme, P., Appourchaux, T., & Boumier, P. 2009, Astronomy and Astrophysics, 506, 7

Handberg, R., & Lund, M. N. 2014, Monthly Notices of the Royal Astronomical Society, 445, 2698

Hekker, S., Broomhall, A.-M., Chaplin, W. J., et al. 2010, MNRAS, 402, 2049

Hekker, S., Elsworth, Y., Mosser, B., et al. 2012, A&A, 544, A90

Høg, E., Fabricius, C., Makarov, V. V., et al. 2000, Astronomy and Astrophysics, 355, L27

Hon, M., Stello, D., García, R. A., et al. 2019, Monthly Notices of the Royal Astronomical Society, 485, 5616

Hon, M., Stello, D., & Yu, J. 2018, Monthly Notices of the Royal Astronomical Society, 476, 3233

Houk, N. 1994, The MK process at 50 years. A powerful tool for astrophysical insight Astronomical Society of the Pacific Conference Series, 60, 285

Huber, D., Stello, D., Bedding, T. R., et al. 2009, Communications in Asteroseismology, 160, 74

Jofré, E., Petrucci, R., Saffe, C., et al. 2015, Astronomy and Astrophysics, 574, A50

Jones, M. I., Jenkins, J. S., Rojo, P., & Melo, C. H. F. 2011, Astronomy and Astrophysics, 536, A71

Kallinger, T., Hekker, S., Mosser, B., et al. 2012, A&A, 541, 51

Luck, R. E. 2015, The Astronomical Journal, 150, 88

Lund, M. N., Handberg, R., Davies, G. R., Chaplin, W. J., & Jones, C. D. 2015, The Astrophysical Journal, 806, 30

Mackereth, J. T., Bovy, J., Leung, H. W., et al. 2019, Monthly Notices of the Royal Astronomical Society, 489, 176

Mathur, S., García, R. A., Régulo, C., et al. 2010, A&A, 511, 46

Meléndez, J., Asplund, M., Alves-Brito, A., et al. 2008, Astronomy and Astrophysics, 484, L21

Miglio, A., Chiappini, C., Morel, T., et al. 2013, Monthly Notices of the Royal Astronomical Society, 429, 423

Mints, A., & Hekker, S. 2018, Astronomy and Astrophysics, 618, A54

Mosser, B., Elsworth, Y., Hekker, S., et al. 2011, Astronomy and Astrophysics, 537, A30

Pinsonneault, M. H., Elsworth, Y. P., Tayar, J., et al. 2018, The Astrophysical Journal Supplement Series, 239, 32

Randich, S., Gratton, R., Pallavicini, R., Pasquini, L., & Carretta, E. 1999, Astronomy and Astrophysics, 348, 487

Ricker, G. R., Winn, J. N., Vanderspek, R., et al. 2015, Journal of Astronomical Telescopes, 1, 014003

Rodrigues, T. S., Bossini, D., Miglio, A., et al. 2017, Monthly Notices of the Royal Astronomical Society, 467, 1433

Sharma, S., Stello, D., Bland-Hawthorn, J., et al. 2019, arXiv e-prints, arXiv:1904.12444

Silva Aguirre, V., Davies, G. R., Basu, S., et al. 2015, Monthly Notices of the Royal Astronomical Society, 452, 2127

Silva Aguirre, V., Bojsen-Hansen, M., Slumstrup, D., et al. 2018, Monthly Notices of the Royal Astronomical Society, 475, 5487

Stello, D., Meibom, S., Gilliland, R. L., et al. 2011, ApJ, 739, 13

Stello, D., Zinn, J., Elsworth, Y., et al. 2017, The Astrophysical Journal, 835, 83

Van Leeuwen, F. 2007, A&A, 474, 653

Wittenmyer, R. A., Liu, F., Wang, L., et al. 2016, The Astronomical Journal, 152, 19

Yıldız, M., Çelik Orhan, Z., & Kayhan, C. 2019, Monthly Notices of the Royal Astronomical Society, 489, 1753

Yu, J., Huber, D., Bedding, T. R., et al. 2018, The Astrophysical Journal Supplement Series, 236, 42

Zinn, J. C., Stello, D., Huber, D., & Sharma, S. 2019, arXiv e-prints, arXiv:1909.11927

Table 1. Measured and derived stellar properties of our targets. The global asteroseismic quantities and stellar properties include a statistical and systematic component derived as described in Sections 3 and 4, respectively. We report them here as $value \pm \sigma_{sta} \pm \sigma_{sys}$.

TIC	$\nu_{\rm max}$ (μHz)	$\Delta\nu$ (μHz)	V (mag)
13097379	$59.10 \pm 1.50 \pm 0.31$	$6.02 \pm 0.03 \pm 0.21$	6.646 ± 0.010
38574220	$29.40 \pm 0.90 \pm 0.25$	$4.06 \pm 0.20 \pm 0.13$	5.577 ± 0.009
38828538	$189.90 \pm 1.60 \pm 0.05$	$14.90 \pm 0.10 \pm 0.06$	5.896 ± 0.009
39082723	$49.30 \pm 2.10 \pm 0.79$	$5.20 \pm 0.10 \pm 0.02$	5.574 ± 0.009
47424090	$28.30 \pm 1.80 \pm 0.82$	$3.40 \pm 0.10 \pm 0.21$	6.930 ± 0.010
70797228	$31.80 \pm 1.50 \pm 0.18$	$4.37 \pm 0.20 \pm 0.22$	5.787 ± 0.009
77116701	$48.30 \pm 7.60 \pm 23.20$	$5.64 \pm 0.20 \pm 3.17$	8.568 ± 0.018
111750740	$142.60 \pm 2.70 \pm 0.22$	$11.80 \pm 0.10 \pm 0.15$	5.658 ± 0.009
115011683	$58.80 \pm 1.20 \pm 0.34$	$6.10 \pm 0.10 \pm 0.00$	6.057 ± 0.010
129649472	$31.80 \pm 1.20 \pm 0.64$	$4.20 \pm 0.20 \pm 0.03$	5.755 ± 0.009
139756492	$27.60 \pm 0.90 \pm 0.07$	$4.16 \pm 0.20 \pm 0.48$	6.819 ± 0.010
141280255	$150.40 \pm 1.00 \pm 0.15$	$12.52 \pm 0.02 \pm 0.08$	5.307 ± 0.009
144335025	$68.50 \pm 1.60 \pm 0.12$	$7.35 \pm 0.20 \pm 0.24$	6.194 ± 0.010
149347992	$165.80 \pm 4.10 \pm 12.54$	$11.10 \pm 0.40 \pm 0.32$	6.405 ± 0.010
155940286	$73.20 \pm 1.30 \pm 0.04$	$7.40 \pm 0.02 \pm 0.09$	6.810 ± 0.010
175375523	$60.00 \pm 1.10 \pm 0.04$	$5.80 \pm 0.10 \pm 0.07$	5.899 ± 0.009
183537408	$57.90 \pm 1.10 \pm 0.26$	$6.20 \pm 0.20 \pm 0.26$	6.781 ± 0.010
204313960	$106.00 \pm 3.30 \pm 0.31$	$9.40 \pm 0.50 \pm 0.16$	6.083 ± 0.010
220517490	$117.30 \pm 1.20 \pm 0.14$	$10.87 \pm 0.02 \pm 0.13$	5.846 ± 0.009
237914586	$47.00 \pm 1.40 \pm 0.53$	$5.74 \pm 0.20 \pm 0.01$	3.959 ± 0.009
270245797	$72.20 \pm 1.70 \pm 0.12$	$6.60 \pm 0.10 \pm 0.19$	6.239 ± 0.009
281597433	$73.30 \pm 1.00 \pm 0.70$	$7.20 \pm 0.03 \pm 0.17$	6.163 ± 0.010
439399563	$44.30 \pm 1.40 \pm 0.15$	$4.54 \pm 0.06 \pm 0.06$	5.892 ± 0.009
441387330	$46.60 \pm 0.80 \pm 0.37$	$5.25 \pm 0.10 \pm 0.17$	5.592 ± 0.009

$T_{\rm eff}$ (K)	[Fe/H] (dex)	R ($R_\odot$)	M ($M_\odot$)	Age (Gyr)	Reference
4634 ± 77	0.04 ± 0.10	$8.49 \pm 0.31 \pm 0.11$	$1.22 \pm 0.09 \pm 0.03$	$6.10 \pm 1.14 \pm 0.71$	Luck (2015)
–	–	–	–	–	–
4828 ± 53	0.11 ± 0.03	$4.68 \pm 0.06 \pm 0.01$	$1.22 \pm 0.03 \pm 0.01$	$6.10 \pm 0.36 \pm 0.11$	Alves et al. (2015)
4706 ± 46	-0.05 ± 0.03	$9.28 \pm 0.14 \pm 0.24$	$1.20 \pm 0.05 \pm 0.08$	$5.90 \pm 0.78 \pm 1.09$	Alves et al. (2015)
–	–	–	–	–	–
4750 ± 100	0.12 ± 0.10	$11.15 \pm 0.77 \pm 0.00$	$1.17 \pm 0.15 \pm 0.03$	$7.10 \pm 2.62 \pm 1.10$	Jones et al. (2011)
–	–	–	–	–	–
4688 ± 100	0.16 ± 0.10	$5.13 \pm 0.16 \pm 0.11$	$1.07 \pm 0.08 \pm 0.08$	$10.60 \pm 1.84 \pm 1.60$	Wittenmyer et al. (2016)
4590 ± 100	-0.13 ± 0.10	$7.94 \pm 0.25 \pm 0.05$	$1.05 \pm 0.08 \pm 0.01$	$9.70 \pm 1.84 \pm 1.62$	Wittenmyer et al. (2016)
4748 ± 42	0.28 ± 0.06	$10.81 \pm 0.31 \pm 0.09$	$1.14 \pm 0.08 \pm 0.01$	$8.30 \pm 1.92 \pm 1.34$	Jofré et al. (2015)
–	–	–	–	–	–
4630 ± 75	0.33 ± 0.03	$5.30 \pm 0.04 \pm 0.02$	$1.23 \pm 0.02 \pm 0.03$	$6.70 \pm 0.36 \pm 0.71$	Meléndez et al. (2008)
–	–	–	–	–	–
5132 ± 50	-0.17 ± 0.09	$7.44 \pm 0.28 \pm 0.27$	$1.99 \pm 0.24 \pm 0.02$	$1.10 \pm 0.32 \pm 0.04$	Randich et al. (1999)
4630 ± 100	0.03 ± 0.10	$6.96 \pm 0.21 \pm 0.18$	$1.01 \pm 0.07 \pm 0.06$	$12.00 \pm 1.92 \pm 1.94$	Wittenmyer et al. (2016)
4660 ± 100	0.26 ± 0.13	$8.99 \pm 0.34 \pm 0.64$	$1.37 \pm 0.11 \pm 0.22$	$4.60 \pm 0.94 \pm 1.37$	Jones et al. (2011)
–	–	–	–	–	–
4897 ± 50	-0.20 ± 0.09	$6.53 \pm 0.17 \pm 0.11$	$1.32 \pm 0.07 \pm 0.05$	$3.70 \pm 0.50 \pm 0.38$	Randich et al. (1999)
4961 ± 24	-0.26 ± 0.02	$5.70 \pm 0.03 \pm 0.01$	$1.14 \pm 0.02 \pm 0.00$	$5.70 \pm 0.36 \pm 0.04$	Alves et al. (2015)
–	–	–	–	–	–
4824 ± 29	-0.10 ± 0.02	$8.80 \pm 0.10 \pm 0.06$	$1.62 \pm 0.04 \pm 0.03$	$2.00 \pm 0.14 \pm 0.07$	Alves et al. (2015)
4700 ± 50	-0.41 ± 0.09	$6.87 \pm 0.17 \pm 0.11$	$0.98 \pm 0.06 \pm 0.04$	$10.30 \pm 1.42 \pm 1.09$	Randich et al. (1999)
4778 ± 59	0.11 ± 0.11	$10.66 \pm 0.33 \pm 0.16$	$1.43 \pm 0.11 \pm 0.07$	$3.50 \pm 0.64 \pm 0.47$	da Silva et al. (2015)
4710 ± 100	-0.02 ± 0.18	$10.04 \pm 0.64 \pm 0.42$	$1.36 \pm 0.17 \pm 0.14$	$3.60 \pm 0.92 \pm 0.63$	Jones et al. (2011)

NOTE—Last column gives the reference from which we retrieved the atmospheric parameters used for the grid-based modelling (see Section 4).